Langmuir

Letter

pubs.acs.org/Langmuir

Resettable Fluorescence Logic Gate Based on Calcein/Layered Double Hydroxide Ultrathin Films

Wenying Shi, Xiaolan Ji, Min Wei,* David G. Evans, and Xue Duan

State Key Laboratory of Chemical Resource Engineering, Beijing University of Chemical Technology, Beijing 100029, P. R. China

Supporting Information

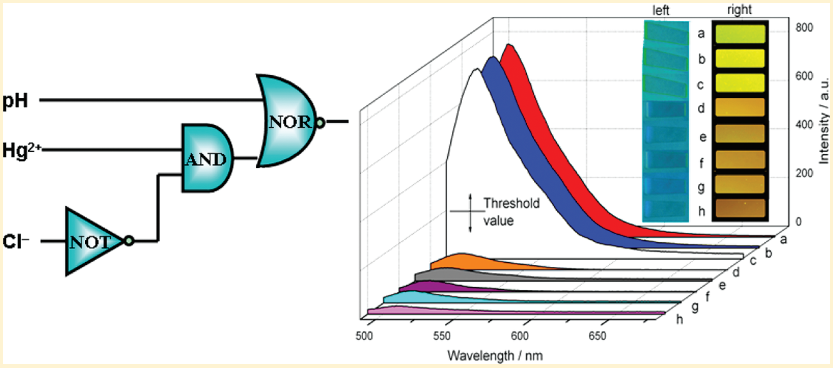

ABSTRACT: A fluorescent logic gate was fabricated based on calcein/layered double hydroxide ultrathin films (UTFs) via alternate assembly technique, which exhibits high stability, reversibility, and resettability. The logic gate was manipulated by utilizing pH value, Hg^{2+} and Cl^- ion as inputs, and the fluorescence emission of the $(calcein/LDH)_{16}$ UTF as output, serving as a three-input logic gate that combines the YES and INHIBIT operation.

1. INTRODUCTION

Miniaturization microprocessors have promoted remarkable improvements in computational capability and speed, in which the design and construction of molecular systems capable of information processing have raised considerable attention.[1] Various molecular systems operating as logic gates can be described using Boolean logic,[2] with the prospect of solving complex problems.[3] From the viewpoint of chemistry, many organic fluorescence molecules have been employed to perform Boolean logic operations due to their detectable fluorescence signal even within one molecule,[4] which results in the remarkable progress of various fluorescence molecule-based logic systems.[5] However, two key problems remain unresolved for the fluorescence molecular logic gates reported previously: (1) they are generally operated in solution, which remains far from practical applications in information technology; (2) unstable lifetime causes signal quenching or drifting, leading to the breakdown of its logic ability in extreme cases. Therefore, how to design advanced fluorescence logic gates still remains a challenging goal.

During the past decade, considerable efforts have been focused on immobilization of fluorescence molecules onto carriers or substrates to develop miniaturized molecule-based gate operation. An important approach is to stablilize fluorescence molecules onto the surface of suitable polymer beads.[6] Unfortunately, polymer-based materials normally suffer from long-term sustainability as a result of variation in illumination, temperature, pressure, environmental pH, and so forth, which limits their practical application. Therefore, one effective solution to this problem is to explore novel matrices for the immobilization of functional fluorescence molecules, for the purpose of achieving gate operations with high stability, reversibility, processability, and resettability.

Layered double hydroxides (LDHs), whose structure can be generally expressed as $[M^{II}_{1-x}M^{III}_x(OH)_2](A^{n-})_{x/n}\cdot mH_2O$ (M^{II} and M^{III} are divalent and trivalent metals respectively; A^{n-} is a n-valent anion), are one type of important layered materials which represent a large versatility in terms of their chemical composition and the ability to build up 2D-organized structures. LDH materials have been widely used in the fields of catalysis, separation, biology, medicine, and sensors.[7] Recently, the delamination of LDHs into nanoscale monolayers which can be used as building blocks for the construction of functional ultrathin films has been widely investigated.[8] This inspires us to challenge the goal of fabricating fluorescence molecular logic gates via alternate assembly of positively charged LDH nanosheets and negatively charged fluorophore by the layer-by-layer (LBL) technique. The combination of fluorescence molecule and this 2D inorganic matrix will show the following advantages: (1) a high dispersion of fluorophore with uniform orientation can be obtained in the confined region of LDH gallery, which would suppress chromophore

Received: March 13, 2012
Revised: April 22, 2012
Published: April 24, 2012

   dx.doi.org/10.1021/la3010739 | Langmuir 2012, 28, 7119−7124

aggregation and reduce fluorescence quenching; (2) a high stability (optical, thermal, and mechanical) for the fluorophore can be achieved due to the presence of inorganic counterpart.

N,*N*-Bis(carboxymethyl)aminomethylfluorescein (calcein, Scheme 1), first reported by Diehl and Ellingboe in 1956,[9] is

Scheme 1. Assembly Process for the (Calcein/LDH)$_n$ UTFs

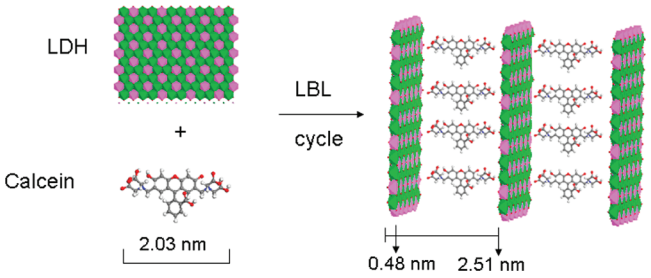

one of the most promising chemical indicators due to its large extinction coefficient, high quantum yield, and acid−base bifunctional property.[10] Herein, fluorescence molecule/LDH UTFs were fabricated by alternate assembly of calcein and ZnAl-LDH nanosheets on quartz substrates using the LBL deposition technique (Scheme 1). The resulting fluorescence UTFs exhibit selective response to pH, Hg^{2+}, as well as Cl^-, which achieves a nanoscale chemical logic gate with a three-input, controllable, and resettable operability.

2. RESULTS AND DISCUSSION

Figure 1A shows the UV−vis absorption spectra of the (calcein/LDH)$_n$ UTFs with various bilayer numbers (n)

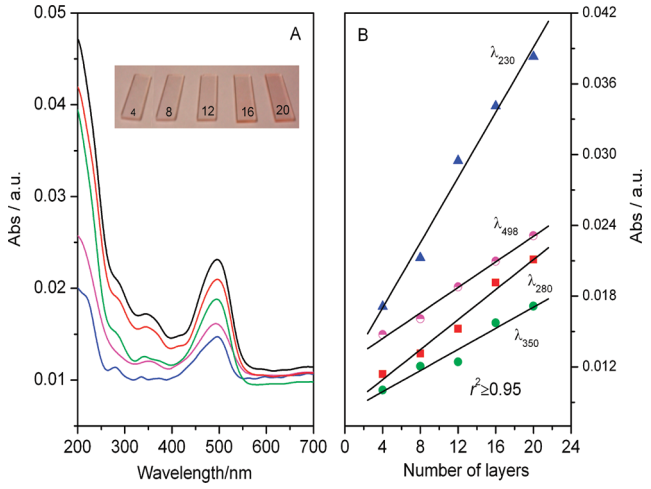

Figure 1. (A) UV−vis absorption spectra of the (calcein/LDH)$_n$ UTFs (n = 4−20) (inset: photographs with different n under daylight); (B) plots of the absorbance at 230, 280, 350, and 498 nm versus n.

deposited on quartz substrates. It was observed that the absorption bands of calcein at ∼230, 280, 350, and 498 nm (π−π^* transition) correlate linearly with n (Figure 1B), indicating a stepwise and regular film growth procedure, which was further confirmed by the gradual color enhancement with the increase of bilayer number (inset in Figure 1A). Compared with the absorption spectrum of pristine calcein solution sample (Figure S1-A, Supporting Information), the absorption band of the (calcein/LDH)$_n$ UTFs becomes broader and unresolved, which may be attributed to the electrostatic interaction between calcein molecule and LDH nanosheets. The fluorescence emission peak at 520 nm of (calcein/LDH)$_n$ UTFs also displays a consistent increase along with n, as shown in Figure S1-B in the Supporting Information. No obvious red or blue shift of the fluorescence spectra for the as-prepared UTFs was observed in comparison with the pristine calcein solution, indicating the absence of calcein aggregation throughout the whole assembly process.

The deposition process of the (calcein/LDH)$_n$ UTFs was further monitored by scanning electron microscopy (SEM; Figure S2-A, Supporting Information). The thicknesses of the as-prepared UTFs (n = 4−16) are in the range 10−43 nm. The approximately linear increase of the thickness upon increasing the layer number confirms that the UTFs present uniform and periodic layered structure (Figure S2-B, Supporting Information), in agreement with the behavior revealed by the absorption and fluorescence spectra above. A typical top view of the SEM image for the (calcein/LDH)$_{16}$ UTF (Figure 2A)

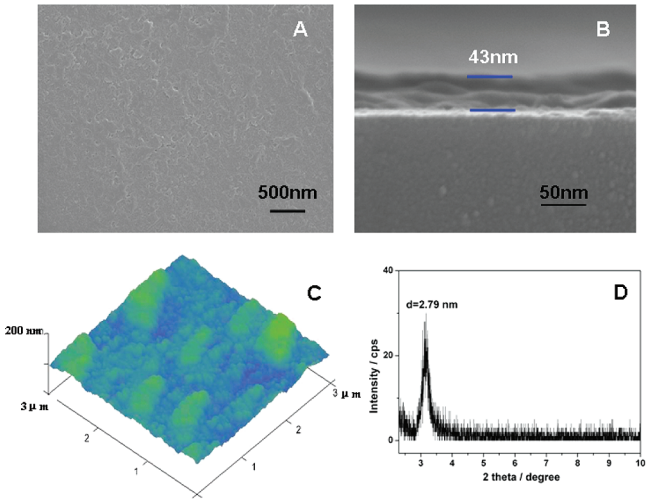

Figure 2. (A) Top-view of SEM image, (B) side-view of SEM image, (C) tapping-mode AFM image, and (D) XRD pattern of the (calcein/LDH)$_{16}$ UTF.

shows that the film surface is microscopically smooth and uniform. The thickness of (calcein/LDH)$_{16}$ UTF is 43 nm observed from its side view of SEM image (Figure 2B), from which it can be estimated that the thickness of one bilayer (calcein/LDH)$_1$ is ∼2.68 nm. The atomic force microscopy (AFM) topographical image (Figure 2C) shows the morphology and roughness information of the UTF, with a root-mean-square roughness of 10.6 nm. The X-ray diffraction (XRD) pattern (Figure 2D) exhibits a Bragg peak at 2θ = 3.16°, indicating a so-called superlattice structure perpendicular to the substrate. The average repeating distance is ∼2.79 nm, approximately consistent with the thickness augment per deposited cycle observed by SEM (2.68 nm). Moreover, this is also in agreement with the ideal single-layered arrangement model of the calcein/LDH supramolecular structure with the thickness of ∼0.48 nm for a monolayer of LDH and 2.03 nm for the extended chain configuration of calcein (Scheme 1).

Taking into account both the fluorescence intensity and response time, the (calcein/LDH)$_{16}$ UTF sample was chosen in the following study (see Figures S1-B, S3 and corresponding discussion, Supporting Information). The pH was used as input

dx.doi.org/10.1021/la3010739 | *Langmuir* 2012, 28, 7119−7124

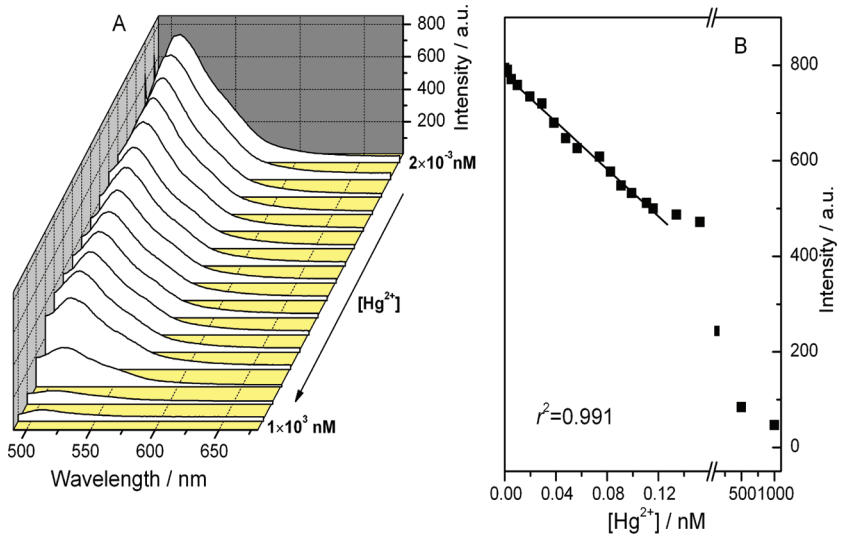

Figure 3. (A) Emission spectra of the $(calcein/LDH)_{16}$ UTF with the presence of different Hg^{2+} concentration (295 K, λ_{ex} = 498 nm); (B) Hg^{2+} titration curve of the $(calcein/LDH)_{16}$ UTF for emission at 510 nm.

for the fluorescence logic gate, which is a fundamental parameter in chemical and biochemical processes. The fluorescence emission spectra and the titration plots for the $(calcein/LDH)_{16}$ UTF with different pH values are shown in Figure S4 (Supporting Information). The fluorescence intensity increases at first to reach a plateau at pH 7.0−8.5 and then gradually decreases as the pH value increases. Calcein displays a complex pH-dependent equilibrium resulting from its various ionic forms (Figure S5, Supporting Information),[11] and the quadrivalent anionic form emits the strongest fluorescence. Therefore, the change in fluorescence intensity of UTFs is based on the equilibrium between different fluorescence forms of calcein in the LDH gallery.

Hg^{2+} also triggers significant change in the fluorescence intensity of the UTF. Figure 3A displays that the fluorescence intensity of the $(calcein/LDH)_{16}$ UTF decreases with the increase of Hg^{2+} concentration from 2.0×10^{-3} nM up to 1.0×10^{3} nM. The titration plot of this UTF obtained with excitation of 498 nm and emission of 510 nm is displayed in Figure 3B. The results show that the fluorescence intensity was proportional to the Hg^{2+} concentration in the range $2.0 \times 10^{-11} \sim 1.2 \times 10^{-10}$ M with r^2 = 0.991. The absolute detection limit was 0.8 pM, much lower than the level defined by the World Health Organization.[12] The reason for fluorescence quenching of the UTF with the presence of Hg^{2+} is related to the binding between calcein and Hg^{2+}, which will be further discussed in the next section.

The fluorescence response of the $(calcein/LDH)_{16}$ UTF to various metal ions (Ca^{2+}, Cd^{2+}, Co^{2+}, Cr^{3+}, Cu^{2+}, K^{+}, Mg^{2+}, Na^{+}, Ni^{2+}, Pb^{2+}, Zn^{2+}, Al^{3+}, and Hg^{2+}) in a neutral medium was investigated (Figure 4A). It was found that the response of the UTF to other cations was much lower compared with Hg^{2+}, and less change in the fluorescence intensity of UTF for these interferential species (∼15%) than Hg^{2+} (∼90%) was observed with the concentration of 1 μM. Moreover, no significant effect on the response of UTF toward Hg^{2+} was found with the presence of all these cations (1 μM each). The results above show that the UTF exhibits a rather high selectivity for Hg^{2+}.

To investigate the effect of anions on the fluorescence of UTF in a neutral medium, the quenched $(calcein/LDH)_{16}$ UTF with Hg^{2+} was immered into a sodium salt solution containing

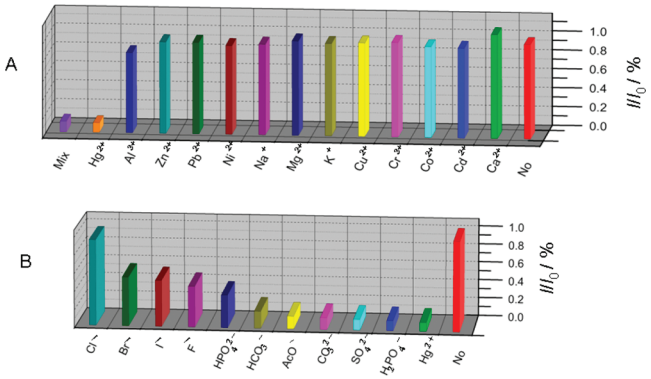

Figure 4. Fluorescence intensity ratio (I/I_0) of the $(calcein/LDH)_{16}$ UTF at 510 nm induced by the indicated: (A) metal cations (1 μM respectively); Mix = a mixed solution containing all the tested cations (1 μM each) and (B) anions (2 μM).

various anions such as $H_2PO_4^-$, SO_4^{2-}, CO_3^{2-}, AcO^-, HCO_3^-, HPO_4^{2-}, F^-, I^-, Br^-, and Cl^- (2 μM each). Significantly, the presence of Cl^- can efficiently recover the fluorescence of the quenched UTF (Figure 4B).

The fluorescence emission spectra, the photographs under UV illumination and microscopic image of the UTFs in the presence of various metal ions, anions as well as with different pH values are shown in Figure 5, from which the following conclusions can be drawn: (1) at high pH value (pH ≥ 12), the fluorescence quenching occurs accompanied with significantly decreased brightness, irrespective of the presence of any metal ions or anions in the system; (2) Hg^{2+} ion can quench the fluorescence of the UTF in the absence of Cl^-; (3) at 6.5 ≤ pH ≤ 12, Cl^- ion can effectively inhibit fluorescence quenching imposed by Hg^{2+}. Based on the above results, we designed a logic device that defines a threshold of pH, Hg^{2+}, and Cl^- as inputs, and the fluorescence signal of the UTF as output. For input, the presence and absence of Hg^{2+} ion (>1 μm) or Cl^- ion (with 2 equiv of Hg^{2+} added) are defined as 1 and 0, respectively; and pH ≥ 12 and 6.5 ≤ pH ≤ 12 as 1 and 0, respectively. For output, the normal fluorescence of the UTF is denoted as 1 and the quenched fluorescence as 0 (see details in Figure 5). Based on the above definitions, binary transfer of a

dx.doi.org/10.1021/la3010739 | Langmuir 2012, 28, 7119−7124

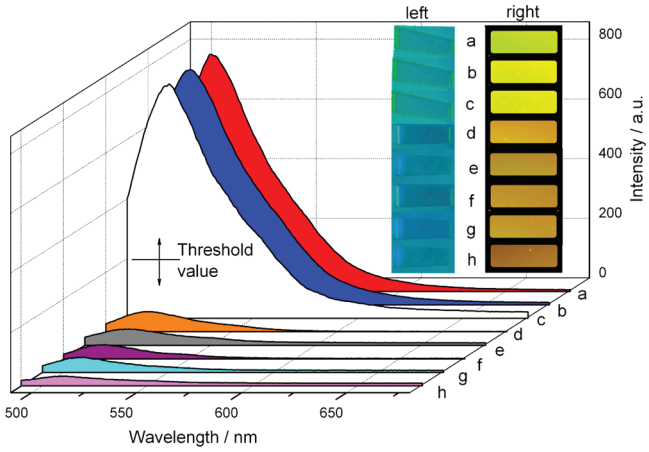

Figure 5. Fluorescence emission spectra [inset: photographs under 365 nm UV light (left) and microscopic images (right)] of the $(calcein/LDH)_{16}$ UTF under different input conditions: a = UTF; b = UTF + Cl^-; c = UTF + Hg^{2+} + Cl^-; d = UTF + OH^- + Cl^-; e = UTF + OH^- + Cl^-+Hg^{2+}; f = UTF + OH^-; g = UTF + Hg^{2+}; h = UTF + OH^- + Hg^{2+}. Fluorescence intensity higher than the threshold value specified at 510 nm is assigned as 1, and lower than that value is assigned as 0.

logic operation can be achieved by controlling the three inputs (pH, Hg^{2+}, Cl^-) and by monitoring the fluorescence output. The truth table and a schematic representation of the logic gate are presented in Table 1. The results show that the $(calcein/LDH)_{16}$ UTF performs the YES and INHIBIT logic operation with the three inputs.

Table 1. Truth Table for the YES and INHIBIT Logic Gate[a]

input 1 pH	input 2 Hg^{2+}	input 3 Cl^-	output F (λ_{em} = 510 nm)
0	0	0	1 (high, 794.9 ± 5)
0	0	1	1 (high, 789.2 ± 8)
0	1	0	0 (low, 67.6 ± 7)
0	1	1	1 (high, 784.8 ± 10)
1	0	0	0 (low, 53.5 ± 5)
1	0	1	0 (low, 49.4 ± 6)
1	1	0	0 (low, 31.9 ± 2)
1	1	1	0 (low, 47.2 ± 3)

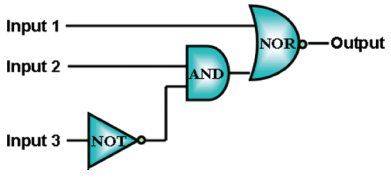

[a]The values in parentheses in the output column indicate the experimental fluorescence intensity in arbitrary units. The corresponding binary states are determined by applying a threshold value of I_F = 200. The errors were determined by repeating experiments for five times.

To develop a better understanding of the mechanism for the logic gate, the X-ray photoelectron spectroscopy (XPS) measurement was recorded (Figure 6). Compared with the original UTF (Figure 6A-a), the XPS spectrum of the UTF + Hg^{2+} sample (Figure 6A-b) displays signal of Hg 4d3 (380.1 eV), indicating that Hg^{2+} was bonded in the UTF via the complexation with calcein. The disappearance of Hg signal for the UTF + Hg^{2+} + Cl^- sample confirms the removal of Hg^{2+}

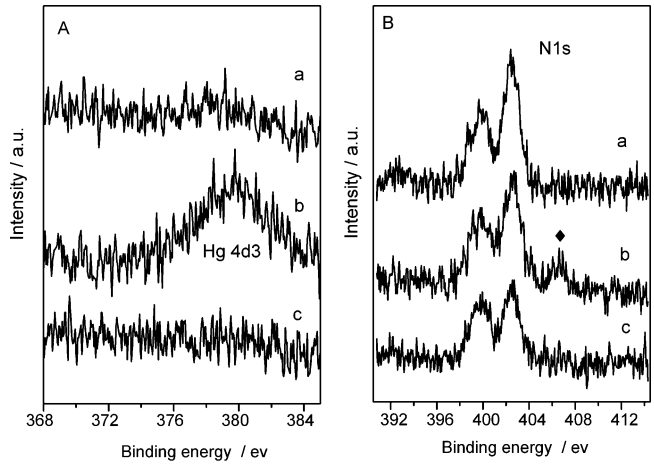

Figure 6. XPS spectra of (A) Hg 4d3 and (B) N 1s: (a) original $(calcein/LDH)_{16}$ UTF, (b) UTF + Hg^{2+}, and (c) UTF + Hg^{2+} + Cl^-.

from the UTF (Figure 6A-c) as a result of the formation of $HgCl_2$ in the solution (the titration plot is shown in Figure S6 in the Supporting Information). The complexation of Hg^{2+} and calcein in the UTF is based on a high thermodynamic affinity of Hg^{2+} for typical N-chelate ligands and fast metal-to-ligand binding kinetics, while the recovery of the quenched UTF is rooted in the complexation of Hg^{2+} and Cl^- due to the much larger complex constant between Cl^- and Hg^{2+} (log $K \approx 13.22$)[13] than calcein and Hg^{2+} (log $K \approx 4.89$ based on the fit result of the Stern−Volmer formula, see Figure S7 in the Supporting Information). The XPS spectra of both the original UTF and the UTF + Hg^{2+} + Cl^- sample show two peaks attributed to N 1s (402.55 and 399.50 eV; 402.60 and 399.65 eV), while the UTF + Hg^{2+} sample displays one new peak at 406.85 eV besides the two old ones, indicating the coordination bond between Hg^{2+} and N atom of calcein (Figure 6B). This new signal of nitrogen with higher binding energy was attributed to the reduction of electron density.[14] Figure S8 in the Supporting Information shows that no change of O and C signals for the original UTF, UTF + Hg^{2+}, and UTF + Hg^{2+} + Cl^- samples was observed, which eliminates the coordination between Hg^{2+} and COO^- groups. In addition, the polarized photoemission spectra show no significant discrepancy in the anisotropy for these three samples, indicating that the embedment/removal of Hg^{2+} does not give rise to effect on orientation and/or stacking of calcein in the gallery of LDH (Figure S9, Supporting Information).

The reset capability is a key factor for the chemical-driven logic operations from the viewpoint of practical application. In this work, the fluorescence can be restored by immersing the quenched $(calcein/LDH)_{16}$ UTF into a solution of EDTA (a metal ion chelator, 10 μM), demonstrating the binding between calcein and Hg^{2+} is chemically reversible. A good repeatability of the UTF was obtained with the RSD = 2.21% (EDTA) and RSD =1.83% (Hg^{2+}) in 20 cycles (Figure S10 in the Supporting Information). This observation suggests that the $(calcein/LDH)_{16}$ UTF logic gate can be readily reset by the treatment of EDTA (Figure S10-A) and/or the adjustment of pH value (Figure S10-B). The liquid-state logic opration generally suffers from the accumulation of chemical waste produced in the reset process. In this work, however, the convenient manipulation of solid-state UTFs effectively resolves this problem in the chemically driven opration process.

dx.doi.org/10.1021/la3010739 | *Langmuir* 2012, 28, 7119−7124

The stability of gate operation is of major importance, since it leads to unreliable and destructive readout and even the breakdown of logic ability. The fluorescence intensity of the $(calcein/LDH)_{16}$ UTF and pristine calcein in solution was recorded by illuminating with UV light for comparison study (Figure S11-A, Supporting Information). A remarkable fluorescence quenching of the calcein solution was observed after 1 h irradiation, while the $(calcein/LDH)_{16}$ UTF remained ~93% of initial fluorescence. The result indicates that the photostability of calcein molecule is significantly enhanced in the LDH matrix. The storage stability test of the UTF shows that ~95.3% of its initial fluorescence intensity remained after 1 month measurement (Figure S11-B). In addition, no delamination or peeling occurred on cross-cutting the surface, indicating strong adhesion of the UTF film to the substrate (shown in Figure S12, Supporting Information).

3. CONCLUSION

In conclusion, a three-input chemically controlled logic gate, which combines the YES and INHIBIT operation, was fabricated by alternate assembly of calcein and Zn−Al LDH nanosheets. The pH value, Hg^{2+}, as well as Cl^- were employed as the three inputs, and the fluorescence intensity of the UTF was monitored as the output. This chemical logic device displays excellent resettability, photostability, as well as mechanical stability. Significantly, the strategy based on the fluorescence molecule/LDH UTFs in this work provides a feasible approach for the fabrication of other integrated, complicated, and multifunctional molecular logic devices. It is anticipated that such intelligent fluorescence molecule/LDH UTF materials can be potentially applied in the fields of environment-sensitive actuators, cell cultures, and molecular switches.

■ ASSOCIATED CONTENT

Supporting Information

Preparation and performance of the $(calcein/LDH)_n$ UTFs; the process of logic gate operation and its stability. This material is available free of charge via the Internet at http://pubs.acs.org.

■ AUTHOR INFORMATION

Corresponding Author

*Telephone: +86-10-64412131. Fax: +86-10-64425385. E-mail: weimin@mail.buct.edu.cn.

Notes

The authors declare no competing financial interest.

■ ACKNOWLEDGMENTS

This project was supported by the National Natural Science Foundation of China, the 973 Program (Grant No.: 2011CBA00504), the Postdoctoral Science Foundation (Grant No.: 20100480183), the Collaboration Project from the Beijing Education Committee, and the Fundamental Research Funds for the Central Universities (Grant No.: ZY1134).

■ REFERENCES

(1) (a) Schultz, M. The End of the Road for Silicon? *Nature* **1999**, *399*, 729. (b) *Springer Handbook of Nanotechnology*; Bhushan, B., Ed.; Springer: Berlin, 2007.

(2) (a) de Silva, A. P.; Seiichi, U. Molecular Logic and Computing. *Nat. Nanotechnol.* **2007**, *2*, 399. (b) Park, K. S.; Jung, C.; Park, H. G. :Illusionary" Polymerase Activity Triggered by Metal Ions: Use for Molecular Logic-Gate Operations. *Angew. Chem., Int. Ed.* **2010**, *49*, 9540. (c) Liu, D.; Chen, W.; Sun, K.; Deng, K.; Zhang, W.; Wang, Z.; Jiang, X. Resettable, Multi-Readout Logic Gates Based on Controllably Reversible Aggregation of Gold Nanoparticles. *Angew. Chem., Int. Ed.* **2011**, *50*, 4103. (d) Cheng, Z.; Jing, Y.; Jin, X. Circular DNA Logic Gates with Strand Displacement. *Langmuir* **2010**, *26*, 1416. (e) Jun, M.; Kenichi, A.; Masaya, M.; Atsushi, A.; Tokuji, M. Quasi-Solid-State Optical Logic Devices Based on Redox Polymer Nanosheet Assembly. *Langmuir* **2009**, *25*, 11061.

(3) (a) de Ruiter, G.; van der Boom, M. E. Surface-Confined Assemblies and Polymers for Molecular Logic. *Acc. Chem. Res.* **2011**, *44*, 563. (b) Marco, F.; Franco, M. Electrochemically Controlled Assembly and Logic Gates Operations of Gold Nanoparticle Arrays. *Langmuir* **2012**, *28*, 3322. (c) Zhang, Z. Y.; Xu, B.; Su, J. H.; Shen, L. P.; Xie, Y. S.; Tian, H. Color-Tunable Solid-State Emission of 2,2′-Biindenyl-Based Fluorophores. *Angew. Chem., Int. Ed.* **2011**, *50*, 11654. (d) Tian, H. Data Processing on a Unimolecular Platform. *Angew. Chem., Int. Ed.* **2010**, *49*, 4710.

(4) (a) Kikkeri, R.; Grunstein, D.; Seeberger, P. H. Lectin Biosensing Using Digital Analysis of Ru(II)-Glycodendrimers. *J. Am. Chem. Soc.* **2010**, *132*, 10230.

(5) (a) Qu, D. H.; Ji, F. Y.; Wang, Q. C.; Tian, H. A Double INHIBIT Logic Gate Employing Configuration and Fluorescence Changes. *Adv. Mater.* **2006**, *18*, 2035. (b) Margulies, D.; Felder, C. E.; Melman, G.; Shanzer, A. A Molecular Keypad Lock: A Photochemical Device Capable of Authorizing Password Entries. *J. Am. Chem. Soc.* **2007**, *129*, 347. (c) Sun, W.; Zhou, C.; Xu, C. H.; Fang, C. J.; Zhang, C.; Li, Z. X.; Yan, C. H. A Fluorescent-Switch-Based Computing Platform in Defending Information Risk. *Chem.—Eur. J.* **2008**, *14*, 6342.

(6) (a) de Silva, A. P.; James, M. R.; Mckinney, B. O. F.; Pears, D. A.; Weir, S. M. Molecular Computational Elements Encode Large Populations of Small Objects. *Nat. Mater.* **2006**, *5*, 787. (b) Matsui, J.; Mitsuishi, M.; Aoki, A.; Miyashita, T. Molecular Optical Gating Devices Based on Polymer Nanosheets Assemblies. *J. Am. Chem. Soc.* **2004**, *126*, 3708.

(7) (a) Fogg, A. M.; Freij, A. J.; Parkinson, G. M. Synthesis and Anion Exchange Chemistry of Rhombohedral Li/Al Layered Double Hydroxides. *Chem. Mater.* **2002**, *14*, 232. (b) Fogg, A. M.; Green, V. M.; Harvey, H. G.; O'Hare, D. New Separation Science Using Shape-Selective Ion Exchange Intercalation Chemistry. *Adv. Mater.* **1999**, *11*, 1466. (c) Wang, X. R.; Lu, J.; Shi, W. Y.; Li, F.; Wei, M.; Evans, D. G.; Duan, X. A Thermochromic Thin Film Based on Host−Guest Interactions in a Layered Double Hydroxide. *Langmuir* **2010**, *26*, 1247.

(8) (a) Han, J. B.; Yan, D. P.; Shi, W. Y.; Ma, J.; Yan, H.; Wei, M.; Evans, D. G.; Duan, X. Layer-by-Layer Ultrathin Films of Azobenzene-Containing Polymer/Layered Double Hydroxides with Reversible Photoresponsive Behavior. *J. Phys. Chem. B* **2010**, *114*, 5678. (b) Liu, Z. P.; Ma, R. Z.; Ebina, Y.; Iyi, N.; Takada, K.; Sasaki, T. General Synthesis and Delamination of Highly Crystalline Transition-Metal-Bearing Layered Double Hydroxides. *Langmuir* **2007**, *23*, 861.

(9) Diehl, H.; Ellingboe, J. L. Indicator for Titration of Calcium in Presence of Magnesium Using Disodium Dihydrogen Ethylenediamine Tetraacetate. *Anal. Chem.* **1956**, *28*, 882.

(10) Kruglenko, I.; Shirshov, Y.; Burlachenko, J.; Savchenko, A.; Kravchenko, S.; Manera, M. G.; Rella, R. Sensitive Coating for Water Vapors Detection Based on Thermally Sputtered Calcein Thin Films. *Talanta* **2010**, *82*, 1392.

(11) (a) Wallach, D. F. H.; Steck, T. L. Fluorescence Techniques in the Microdetermination of Metals in Biological Materials. Utility of 2,4-Bis-[*N*,*N*′-di-(carboxymethyl)aminomethyl] Fluorescein in the Fluorometric Estimation of Al^{+3}, Alkaline Earths, Co^{+2}, Cu^{+2}, Ni^{+2}, and Zn^{+2} in Micromolar Concentrations. *Anal. Chem.* **1963**, *35*, 1035. (b) Wallach, D. F. H.; Surgenor, D. M.; Soderberg, J.; Delano, E. Preparation and Properties of 3,6-Dihydroxy-2,4-bis-[*N*-*N*′-di-(carboxymethyl)-aminomethyl] fluoran. *Anal. Chem.* **1959**, *31*, 456.

(12) World Health Organization. *Guidelines for drinking-water quality: incorporating 1st and 2nd addenda*, Recommendations, 3rd ed.; World

Health Organization: Geneva, 2008, Vol. *1*, http://www.who.int/water_sanitation_health/dwq/fulltext.pdf (accessed November 10, 2010).

(13) Dean, J. A. *Lange's Handbook of Chemistry*, 15th ed.; Science Press and McGraw-Hill Education: Asia, 1998.

(14) (a) McPhail, M. R.; Sells, J. A.; He, Z. C.; Chusuei, C. Charging Nanowalls: Adjusting the Carbon Nanotube Isoelectric Point via Surface Functionalization. *J. Phys. Chem. C* **2009**, *113*, 14102. (b) Wu, J. B.; Lin, Y. F.; Wang, J. L.; Chang, P. J.; Tasi, C. P.; Lu, C. C.; Chiu, H. T.; Yang, Y. W. Correlation between N 1s XPS Binding Energy and Bond Distance in Metal Amido, Imido, and Nitrido Complexes. *Inorg. Chem.* **2003**, *42*, 4516.